**Article:**

Ardestani, MM, Moazen, M and Jin, Z (2015) Contribution of geometric design parameters to knee implant performance: Conflicting impact of conformity on kinematics and contact mechanics. Knee, 22 (3). pp. 217-224. ISSN 0968-0160

https://doi.org/10.1016/j.knee.2015.02.011

**Original article**

# Contribution of geometric design parameters to knee implant performance: conflicting impact of conformity on kinematics and contact mechanics

Marzieh M. Ardestani[1,*], Mehran Moazen[2], Yang Wenjian[1], and Zhongmin Jin [1, 3]

[1]State Key Laboratory for Manufacturing System Engineering, School of Mechanical Engineering, Xi'an Jiaotong University, Xi'an, China

[2]Medical and Biological Engineering, School of Engineering, University of Hull, Hull, UK

[3]Institute of Medical and Biological Engineering, School of Mechanical Engineering, University of Leeds, UK

**□*Corresponding author (M.M.Ardestani) Tel.: +0-86-029-83395122;**

**E-mail: mostafavizadeh@yahoo.com**

**Abstract:**

**Background:** Outcomes of total knee arthroplasty are closely related to articular geometry of implanted prostheses. Geometry has a competing effect on kinematics and contact mechanics of prosthetic knee such that an implant geometry that generates lower contact pressure will impose more constraints on knee kinematics. The geometric parameters that may cause this competing effect have not been well understood. This study aimed to quantify the underlying causal relationships between implant geometric variables and its performance metrics.

**Methods:** Parametric dimensions of a fixed-bearing cruciate retaining implant were randomized to produce a number of perturbed implant geometries. Performance metrics (i.e. maximum contact pressure and kinematic range of motion) of each randomized implant were calculated using finite element method and artificial neural network technique. The relative contributions of individual geometric variables to the performance metrics were then determined through principal component analysis (PCA).

**Results:** Results showed that femoral and tibial distal radii, femoral and tibial posterior radii and femoral frontal radius are the most important key parameters which might cause the conflicting impact of geometry on its kinematics and contact mechanics. In the sagittal plane, distal radii of femur and tibia affected both contact pressure and anterior-posterior displacement of the prosthetic components. Also, posterior radii of femur and tibia influenced both contact pressure and internal-external rotation of the prosthetic knee. In the frontal plane, femoral frontal radius influenced both contact pressure and internal-external rotation of the prosthetic components.

**Conclusion:** Such investigations can be used to potentially enhance the future knee implant designs.

**Keywords：** Total knee arthroplasty, Kinematics, Contact mechanics, Finite element simulation, Artificial neural network

## 1. Introduction

Knee implant geometry directly affects the outcome of total knee arthroplasty [1-9]. It affects both contact mechanics [4, 10-13] and kinematics of the articulating components [14-19] . In fact, implant geometry has a competing effect on the resultant kinematics and contact mechanics [20, 21]. For instance, a high conformity design which decreases the contact pressure at the articulating surfaces may restrict the relative displacement of the prosthetic components that adversely affects the kinematics [10].

Previous computational attempts have investigated the impact of implant geometry on its kinematics [22] and contact mechanics [10, 23-25]. However, to best of our knowledge, no previous study has quantified the underlying causal relationships between implant geometry and its performance metrics (kinematics and contact mechanics). A key rationale behind lack of such studies is perhaps high computational cost of iterative finite element (FE) simulations that are required. Moreover, discriminating between the contributions of individual geometric variables is challenging as geometric variables are highly coupled to each other and all geometric variables "jointly" contribute to dictate the overall performance of a knee implant [20].

Artificial neural network (ANN) and principal component analysis (PCA) are two powerful methods that can reduce the computational cost of iterative FE models. Artificial neural network (ANN) is an efficient surrogate model with the ability to "learn" a nonlinear relationship [26]. Once a set of inputs and corresponding outputs are presented to the network, the network learns the causal interactions between inputs and outputs. Given a new set of inputs, the trained neural network (surrogate model) can generalize the relationship and calculate the associated outputs. The ANN surrogate therefore can release the necessity of repeating computationally expensive FE models. For example, ANN has been used in conjunction with FE analysis to predict contact mechanics [27, 28], wear and tribological behavior [29], joint load distribution [30, 31] and bone tissue adaption [32-34]. On the other hand, PCA can model complicated interactions between input variables and output metrics in terms of relative contribution [35]. PCA transfers a complicated data space of inputs and corresponding outputs to a secondary orthogonal data space in which important modes of variations can be extracted and analyzed.

The present study aimed to quantify the causal relationship between knee implant geometry and its resultant performance metrics using a combined ANN, PCA and FE analysis. The implant performance was outlined in terms of maximum contact pressure and kinematic range of motions (i.e. anterior-posterior range of displacement and internal-external range of rotation). Using FE and ANN, the aforementioned performance metrics were calculated for a number of probabilistic geometries. The relative contributions of individual geometric variables to the overall implant function were then evaluated through PCA. Such investigations enlighten the competing effect of implant geometry on its performance metrics and can potentially lead towards optimized implant designs.

## 2. Materials and methods

Femoral and tibial insert geometry of a knee replacement implant were parameterized and randomized to generate a wide range of implant geometries (section 2.1). A number of these randomized geometries were analyzed using FE method to calculate the (1) maximum contact pressure, (2) anterior-posterior range of displacement and (3) internal-external range of rotation (section 2.2). A feed forward artificial neural network (FFANN) was then trained to learn the nonlinear relationship between geometric variables as inputs and the corresponding performance metrics as outputs. The trained network then predicted the performance metrics, corresponding to the remaining randomized implant geometries (section 2.3). The contributions of individual geometric parameters to the overall implant performance were quantified using PCA (section 2.4).

### 2.1. Parametric tibiofemoral models

A computer aided design (CAD) model of a fixed-bearing cruciate retaining knee implant was created in CATIA software (V.5, Dassault Systemes, MA, USA). Femoral and tibial dimensions of the model were parameterized through a total number of sixteen geometric variables associated with the medial and lateral femoral and tibial components (Table 1 and Figure 1). The allowable upper and lower boundaries of each design variable were obtained from literature [21]. Each design variable was then randomized from a uniform distribution based on Latin hyper cube sampling (LHS) technique. In LHS technique, the sampling space of each variable was divided into equal-probability intervals and one sample was chosen from each interval to ensure an equal coverage of the whole sampling space [36].

### 2.2. Finite element simulation

A total number of 256 "critical" candidates, built from the minimum and maximum values of the geometric variables, were imported into the commercial finite element package (ABAQUS/Explicit, V6.12 Simulia Inc., RI, USA). Each tibiofemoral knee implant consisted of two main parts; femoral component and tibia insert. Rigid body assumptions were applied to both femoral and tibial insert components, with a simple linear elastic foundation model defined between the two contacting bodies [37]. Tetrahedral (C3D10M) elements were used to mesh the tibiofemoral knee implants in ABAQUS. Convergence was tested by decreasing the edge length of elements from 8 mm to 0.5 mm in five steps (8, 4, 2, 1,and 0.5 mm). The solution converged on the parameter of the interest (⩽ 5% - contact pressure) with over 86000 elements depending on the dimensions of the candidate femoral and tibial components. Penalty based contact condition was specified at the tibia insert and femoral component interface with a friction coefficient of 0.04 [37].

Kinematics and contact mechanics were calculated based on a computational model of Stanmore knee simulator [38-41]. Stanmore simulator is a well-established load-controlled knee simulator in which in vivo environment of knee joint is replicated through applying forces and moments to femoral and tibial components [42, 43]. Soft tissue constraints were modeled with mechanical spring-based assembly consisted of four linear springs [38, 41] (Figure 2). The loading and boundary conditions were obtained from a load-controlled protocol, consistent with ISO Standard 14243-2 [44]: (1) tibia insert was free in medial-lateral direction while it was constrained in superior-inferior, flexion-extension and valgus-varus directions. Anterior-posterior (AP) force and internal-external (IE) torque were applied to the tibia insert; (2) femoral component was free in valgus-varus direction while it was constrained in anterior-posterior, medial-lateral and internal-external directions. Flexion angle and axial load were applied to the femoral component. The required boundary condition (flexion angle) and load profiles (axial force, AP force, and IE torque) were obtained from a normal gait cycle similar to our previous study [28, 45] (Figure 3a). The contact pressure and kinematics were calculated over the whole flexion cycle. In this study, only maximum contact pressure and kinematic range of motion (ROM) including anterior-posterior range of displacement (A-P ROM) and internal-external range of rotation (I-E ROM) were reported (Figure 3b) .

### 2.3. Artificial neural network surrogate

Feed forward artificial neural network (FFANN) is a well-known approximator [28, 45-47], capable of learning any nonlinear relationship between inputs and outputs regardless of their complexity [48]. A three-layer FFANN with one input layer, one hidden layer and one output layer was constructed (Figure 4). This structure had sixteen inputs (geometric variables, see Figure 1) and three outputs (maximum contact pressure, A-P ROM and I-E ROM, see Figure 3b). Details of this neural network can be found in our previous studies [28, 45-47] . In brief, hidden neurons were activated by "hyperbolic tangent sigmoid" function and output nodes were activated with a "pure line" function to produce a weighted sum of hidden neurons in the output. The aforementioned 256 randomized geometries and their associated performance metrics, computed through FE models, served as the training data space for the neural network. This data space was randomly divided into three distinguished subsets: train (70%), validation (15%) and test (15%). Train and validation subsets were used to train the network and adjust the connection weights through a gradient descent back propagation algorithm with an adaptive learning rate. Validation subset was used to evaluate the "prediction accuracy" of the trained network, whilst test subset was mainly used to assess the "generalization ability" of the trained structure for new sets of inputs. "Prediction accuracy" was defined as the normalized root mean square error between FFANN predictions and FE computations. "Generalization ability" was defined as the percentage of the test data space that was accurately predicted by the FFANN. In brief, there was a trade-off between "prediction accuracy" of the network and its "generalization ability". Both generality and accuracy of the network were in turn affected by the number of hidden neurons and the error goal, used in the training procedure. A precise error goal or more number of hidden neurons adjusted the weights precisely and increased the accuracy of the network. However, too many hidden neurons or a rigorous error goal decreased the generality of the trained network due to over-fitting and yielded to an increase in the prediction error on the test subset [49]. A number of different hidden neurons (5 to 30 neurons with an increment of 5 neurons in each step) and a variety of different error goal values (Err=0.01 Err=0.05 Err=0.1 Err=0.2) were examined to find the best compromised network. This network was then used to calculate the performance metrics (outputs) of the remaining perturbed geometries (inputs).

### 2.4. Principal component analysis

In general, the overall performance of an implant is dictated through a complex interaction between geometric variables [10, 20-22, 24, 25]. Traditional sensitivity analysis however, often discards the complex inter-dependencies between input variables [35]. Instead, PCA was employed to investigate the causal relationship between geometric variables of the implant and its performance [50]. The probabilistic geometries and the corresponding performance metrics were arranged in a matrix T:

$$T = [\text{Sixteen geometric design variables , performance measurs}] \quad (1)$$

In the above matrix, each row demonstrates one candidate implant and its performance metrics. Matrix T was transferred into an orthogonal data space of PC values:

$$\text{PC value} = T \times E_T \quad (2)$$

Where $E_T$ is a feature matrix consisted of all eigenvectors of matrix T. PC values were in fact the secondary "independent" variables for the primary "inter-dependent" variables (geometric variables and performance metrics). Each PC value consisted of two parts: one part was related to the geometric variables and the other was related to the performance metrics. The first part represented how the geometric variables varied together and the second explained how the resultant performance metrics were changed accordingly. The normalized ratio of PC values corresponding to the "geometric variables" to the PC values associated with the "performance metrics" were interpreted as relative contribution (RC) indices of geometric variables to the implant function ($0 \leqslant RC \leqslant 1$).

## 3. Results

The geometric variables were randomly sampled and a total number of 500 probabilistic tibiofemoral designs were created. For a number of 256 candidate designs, kinematics and contact mechanics were computed using FE simulation (Figure 5). The simulation time for a complete gait cycle, discretized into 100 increments, was approximately 40 minutes for each FE model on a dual core CPU (2.93GHz, 4GB RAM). The performance metrics were then outlined through the maximum contact pressure, A-P ROM and I-E ROM. A three-layer FFANN, with sixteen geometric variables as inputs and three performance metrics as outputs, was trained based on FE computations. Table 2 summarizes the performance of this network for different numbers of hidden neurons and a variety of error goal values. It was found that the more precise the error goal was, the more epochs were needed to train the network. More training epochs in turn yielded to a network with lower generality. For example, for the error goal of Err=0.01, training epochs ranged from 800 to 1200 and generality varied from 36% to 54%. For an error goal of Err=0.1 however, lower numbers of training epochs were needed (498 to 660) and the generality ranged from 90% to 100%. Also, with a precise error goal (Err=0.01 and 0.05), increasing the number of hidden neurons necessitated further number of training epochs. Although the prediction accuracy was increased, the generality was adversely decreased due to over-fitting.

On the other hand, with a flexible error goal (Err=0.1 and 0.2), increasing the number of hidden neurons enhanced both prediction accuracy and generality of the trained network. Table 2 demonstrates that the proposed FFANN with the error goal of Err=0.1 and fifteen hidden neurons achieved the best compromise between accuracy and generality. Thus this network was used to estimate the performance metrics of the remaining geometries. The simulation time of the trained FFANN, to produce an estimation of implant performance metrics for each set of geometric variables, was approximately 30 sec on the same CPU.

The relative contribution indices, obtained from PCA, discriminated between contributions of different individual geometric variables to the performance metrics (Figure 6). Results highlight that contact pressure was significantly more sensitive to the variations in the tibia frontal radius ($RC^{\text{contact pressure}}_{\text{tibia frontal}} = 0.70$), tibia distal radius ($RC^{\text{contact pressure}}_{\text{tibia distal}} = 0.65$) and femoral distal radius ($RC^{\text{contact pressure}}_{\text{femoral distal}} = 0.57$) than to variations in other geometric variables. A-P ROM was sensitive to the femoral posterior radius ($RC^{\text{A-P ROM}}_{\text{femoral posterior}} = 0.64$), femoral distal radius ($RC^{\text{A-P ROM}}_{\text{femoral distal}} = 0.58$), and tibia distal radius ($RC^{\text{A-P ROM}}_{\text{tibia distal}} = 0.60$). I-E ROM was slightly more sensitive to the femoral posterior radius ($RC^{\text{I-E ROM}}_{\text{femoral posterior}} = 0.72$), tibia posterior radius ($RC^{\text{I-E ROM}}_{\text{tibia posterior}} = 0.58$) and tibia anterior radius ($RC^{\text{I-E ROM}}_{\text{tibia anterior}} = 0.58$) than to the femoral frontal ($RC^{\text{I-E ROM}}_{\text{femoral frontal}} = 0.35$) or tibia frontal ($RC^{\text{I-E ROM}}_{\text{tibia frontal}} = 0.10$) radii. Results also demonstrate that the distal radii of femur and tibia have a higher impact on both contact pressure and A-P ROM, than their posterior radii. Posterior radii of femur and tibia in turn simultaneously affected both contact pressure and I-R ROM. These geometric variables therefore might cause the conflicting effect of sagittal conformity on the implant kinematics and contact mechanics. Similarly, femoral frontal radius contributes to the conflicting effect of the frontal conformity since both I-E rotation and contact mechanics were related to this geometric variable.

## 4. Discussion

### 4.1. Neural network surrogate model

Ideally, all of the randomized implant geometries should be evaluated using FE method. However, FE simulation is computationally expensive which makes it impractical to be used iteratively for hundred numbers of randomized implant geometries. A neural network (surrogate model) was therefore trained using

FE computations to learn the causal relationship between geometric variables (inputs) and implant function (outputs). To build the initial training data base, required to train the FFANN surrogate, a total of 256 FE simulations were performed. It should be pointed out that similar to any other kind of surrogate models, the proposed neural network required some initial computational cost to establish the training data base through running the original FE model. However, once the FFAMM trained, it generalized the underlying causal relationship to further numbers of randomized geometries and released the necessity of repeating the FE simulation. It therefore facilitated the simulation of hundreds implant geometries in a fraction of the time required for running the original FE model (30 seconds compared to 40 minutes for each perturbed geometry). It should be pointed out that although a trained FFANN can generalize the causal relationship to new implant geometries, FFANN can only interpolate the training examples. In other words, predictions of FFANN are accurate and valid for those inputs which lay within the training data base. In the present study, the proposed FFANN was trained using the FE computations of those candidate implants which were built from the minimum and maximum values of the geometric variables (critical candidates).

### 4.2. Validation

Overall, the general trends of finite element computations were well compared with the previously published experimental and computational literature for the fixed-bearing cruciate retaining implants [38-41]. Beside this, computational findings are in a good agreement with previous studies which in turn reassures the reliability of the proposed computational framework: first, frontal conformity, defined by the femoral frontal, tibia frontal and condylar space, had a higher contribution to the contact pressure than to the kinematics ( $RC^{\text{contact pressure}}_{\text{frontal conformity}}$ = 0.41 vs. $RC^{\text{kinematics}}_{\text{frontal conformity}}$ = 0.13) (Sathasivam and Walker, 1999); second, results highlighted the key impact of the tibia frontal radius on the condylar contact pressure ( $RC^{\text{contact pressure}}_{\text{tibia frontal}}$ = 0.73), and the relative contribution of the femoral posterior radius to the kinematic variations ( $RC^{\text{kinematics}}_{\text{feomral posterior}}$ = 0.68) (Fitzpatrick et al., 2012a, Fitzpatrick et al., 2012b).

### 4.3. Contribution of the present study

Previous studies have mostly described the condylar shape of the knee implant in terms of conformity. Although, the competing effect of conformity on the implant kinematics and contact mechanics has been well understood [10, 20, 21], the geometric variables which may cause this competing relationship have not been studied in a systematic manner. The present study developed a computational framework to provide further insights into this conflicting relationship. Contribution indices demonstrated that femoral and tibial distal radii, femoral and tibial posterior radii and femoral frontal radius are the most important key parameters which might cause the conflicting impact of conformity on performance metrics (see Figure 6). In the sagittal plane, femoral and tibial distal radii affected both contact pressure and AP displacement of the prosthetic components. Also, femoral and tibial posterior radii concurrently affected contact pressure and IE rotation of the prosthetic components. In the frontal plane, femoral frontal radius influenced both contact pressure and IE rotation of the prosthetic components.

Findings of this study can be used to potentially enhance the future knee implant designs. For instance, present findings suggested that femoral posterior radius affected the kinematics more than the contact mechanics ( $RC^{\text{kinematics}}_{\text{femoral posterior}}$ = 0.70 vs. $RC^{\text{contact pressure}}_{\text{femoral posterior}}$ = 0.30). Accordingly, a reduction in the conformity achieved via femoral posterior radius may enhance kinematics of the knee implant whilst its adverse effect on the contact pressure may still be tolerated. Similarly, increasing the frontal conformity via tibia frontal radius may reduce the contact pressure with the minimum adverse effect on the implant kinematics ( $RC^{\text{contact pressure}}_{\text{tibia frontal}}$ = 0.73 vs. $RC^{\text{kinematics}}_{\text{tibia frontal}}$ = 0.1).

This perspective may also provide potential benefits for patient-specific designs. For example, an active golf athlete who demands higher levels of knee rotation may take advantage of a less constraint implant that is specifically designed over femoral posterior (FP) , tibia posterior (TP) and tibia anterior(TA) radii with more influence on I-E rotation than contact pressure ( $RC^{\text{I-E ROM}}_{\text{FP,TP,TA}}$ = 0.63 vs. $RC^{\text{contact pressure}}_{\text{FP,TP,TA}}$ = 0.25). On the other hand an elderly patient with less physical activity who demands more durability may benefit from a more constraint design that is achieved over tibia frontal radius with minimum adverse effect on kinematics ( $RC^{\text{contact pressure}}_{\text{tibia frontal}}$ = 0.73 vs. $RC^{\text{kinematics}}_{\text{tibia frontal}}$ = 0.1).

### 4.4. Limitations and future research direction

There were several limitations in this study: (1) rigid body constraints were applied to both femoral and tibial components. Halloran et al (2005) showed that rigid body analysis of the tibiofemoral knee implant can calculate contact pressure in an acceptable consistence with a full deformable model whilst rigid body analysis would be much more time-efficient. Therefore, in order to produce the training data base, required to train the neural network, rigid body constraints were applied; (2) contact mechanics of knee implants were outlined as contact pressure. However, wear should be considered as a more rigorous tribological metric [4]. Wear is a function of kinematics and contact mechanics [51] and wear estimation requires more computational effort. Nevertheless, the proposed methodology should be equally applicable to investigate the causal relationship between geometric variables and wear; (3) although computational findings were in a good agreement with the available literature [20, 52, 53], part of the presented findings has not been reported elsewhere and further clinical investigations are required to test whether changes in the proposed dimensions can alleviate the competing effect of implant geometry on its performance metrics. Accordingly, various future directions from this study can be considered: (1): on the methodological level, more tribological metrics (e.g. wear) can be included into the computational framework; (2) on the validation level, a 3D printer can be used to print different tibiofemoral components for testing in an in vitro set-up. It is expected that increasing the conformity via changes in the in the femoral and tibial distal radii leads to higher adverse effects on the implant constraints (due to simultaneous impact on contact pressure and kinematics) compared to a high conformity design which is achieved through changes in tibia frontal radius.

**Conflict of interest statement**

The authors have no conflict of interests to be declared.

**Acknowledgments**

This work was supported by “The Fundamental Research Funds for the Central Universities”, National Natural Science Foundation of China [E050702]，the program of Xi’an Jiao Tong University [grant number xjj2012108], and the program of Kaifang funding of the State Key Lab for Manufacturing Systems Engineering [grant number sklms 2011001].

## References

[1] B.C. Carr, T. Goswami, Knee implants – Review of models and biomechanics, Materials & Design, 30 (2009) 398-413.

[2] C.W. Clary, C.K. Fitzpatrick, L.P. Maletsky, P.J. Rullkoetter, The influence of total knee arthroplasty geometry on mid-flexion stability: An experimental and finite element study, Journal of biomechanics, 46 (2013) 1351-1357.

[3] D.A. Dennis, R.D. Heekin, C.R. Clark, J.A. Murphy, T.L. O'Dell, K.A. Dwyer, Effect of Implant Design on Knee Flexion, The Journal of Arthroplasty, 28 (2013) 429-438.

[4] A. Essner, R. Klein, M. Bushelow, A. Wang, M. Kvitnitsky, O. Mahoney, The effect of sagittal conformity on knee wear, Wear, 255 (2003) 1085-1092.

[5] C.K. Fitzpatrick, P.J. Rullkoetter, Influence of patellofemoral articular geometry and material on mechanics of the unresurfaced patella, Journal of Biomechanics, 45 (2012) 1909-1915.

[6] O.M. Mahoney, C.D. McClung, T.P. Schmalzried, The effect of total knee arthroplasty design on extensor mechanism function, The Journal of arthroplasty, 17 (2002) 416-421.

[7] Morra. E, Postak. P.D, A.S. Greenwald, The effects of articular geometry on delamination and pitting of UHMWPE tibial inserts : a finite element study, Orthopedic research laboratories, (1996).

[8] P.S. Walker, Application of a novel design method for knee replacements to achieve normal mechanics, The Knee, (2012).

[9] P.S. Walker, M.T. Lowry, A. Kumar, The Effect of Geometric Variations in Posterior-stabilized Knee Designs on Motion Characteristics Measured in a Knee Loading Machine, Clinical Orthopaedics and Related Research®, 472 (2014) 238-247.

[10] B.J. Fregly, C. Marquez-Barrientos, S.A. Banks, J.D. DesJardins, Increased conformity offers diminishing returns for reducing total knee replacement wear, Journal of biomechanical engineering, 132 (2010) 021007.

[11] Haider. H, Schroeder. D, Metzger.R, G. K.L, Force control simulation discriminates wear due to small differences in TKR design 52nd Annual Meeting of the Orthopaedic Research Society, (2006).

[12] R.D. Komistek, R.D. Scott, D.A. Dennis, D. Yasgur, D.T. Anderson, M.E. Hajner, < i> In vivo</i> comparison of femorotibial contact positions for Press-Fit posterior stabilized and posterior cruciate [ndash] retaining total knee arthroplasties, The Journal of arthroplasty, 17 (2002) 209-216.

[13] J.J. Rawlinson, D.L. Bartel, Flat medial–lateral conformity in total knee replacements does not minimize contact stresses, Journal of Biomechanics, 35 (2002) 27-34.

[14] A. Burton, S. Williams, C.L. Brockett, J. Fisher, In Vitro Comparison of Fixed- and Mobile Meniscal–Bearing Unicondylar Knee Arthroplasties: Effect of Design, Kinematics, and Condylar Liftoff, The Journal of Arthroplasty, 27 (2012) 1452-1459.

[15] H.E. Cates, R.D. Komistek, M.R. Mahfouz, M.A. Schmidt, M. Anderle, In Vivo Comparison of Knee Kinematics for Subjects Having Either a Posterior Stabilized or Cruciate Retaining High-Flexion Total Knee Arthroplasty, The Journal of Arthroplasty, 23 (2008) 1057-1067.

[16] K.M. Coughlin, S.J. Incavo, R.R. Doohen, K. Gamada, S. Banks, B.D. Beynnon, Kneeling Kinematics After Total Knee Arthroplasty: Anterior-Posterior Contact Position of a Standard and a High-Flex Tibial Insert Design, The Journal of Arthroplasty, 22 (2007) 160-165.

[17] G.R. Klein, J. Parvizi, V.R. Rapuri, M.S. Austin, W.J. Hozack, The effect of tibial polyethylene insert design on range of motion: Evaluation of in vivo knee kinematics by a computerized navigation system during total knee arthroplasty, The Journal of Arthroplasty, 19 (2004) 986-991.

[18] G.R. Klein, C. Restrepo, W.J. Hozack, The Effect of Knee Component Design Changes on Range of Motion: Evaluation In Vivo by a Computerized Navigation System, The Journal of Arthroplasty, 21 (2006) 623-627.

[19] S. Pianigiani, Y. Chevalier, L. Labey, V. Pascale, B. Innocenti, Tibio-femoral kinematics in different total knee

arthroplasty designs during a loaded squat: A numerical sensitivity study, Journal of biomechanics, 45 (2012) 2315-2323.

[20] S. Sathasivam, P. Walker, The conflicting requirements of laxity and conformity in total knee replacement, Journal of biomechanics, 32 (1999) 239-247.

[21] R. Willing, I.Y. Kim, Quantifying the competing relationship between durability and kinematics of total knee replacements using multiobjective design optimization and validated computational models, Journal of biomechanics, 45 (2012) 141-147.

[22] R. Willing, I.Y. Kim, Design optimization of a total knee replacement for improved constraint and flexion kinematics, Journal of biomechanics, 44 (2011) 1014-1020.

[23] J. Dargahi, S. Najarian, S. Amiri, Optimization of the geometry of total knee implant in the sagittal plane using FEA, Bio-medical materials and engineering, 13 (2003) 439-449.

[24] S. Sathasivam, P.S. Walker, Optimization of the bearing surface geometry of total knees, Journal of biomechanics, 27 (1994) 255-264.

[25] R. Willing, I.Y. Kim, Three dimensional shape optimization of total knee replacements for reduced wear, Structural and Multidisciplinary Optimization, 38 (2009) 405-414.

[26] S.S. Haykin, S.S. Haykin, S.S. Haykin, S.S. Haykin, Neural networks and learning machines (Prentice Hall New York, 2009).

[27] Y. Lu, P.R. Pulasani, R. Derakhshani, T.M. Guess, Application of neural networks for the prediction of cartilage stress in a musculoskeletal system, Biomedical Signal Processing and Control, 8 (2013) 475-482.

[28] M.M. Ardestani, M. Moazen, Z. Jin, Gait modification and optimization using neural network–genetic algorithm approach: Application to knee rehabilitation, Expert Systems with Applications, 41 (2014) 7466-7477.

[29] M. Hayajneh, A.M. Hassan, A. Alrashdan, A.T. Mayyas, Prediction of tribological behavior of aluminum–copper based composite using artificial neural network, Journal of Alloys and Compounds, 470 (2009) 584-588.

[30] G. Campoli, H. Weinans, A.A. Zadpoor, Computational load estimation of the femur, Journal of the Mechanical Behavior of Biomedical Materials, 10 (2012) 108-119.

[31] A.A. Zadpoor, G. Campoli, H. Weinans, Neural network prediction of load from the morphology of trabecular bone, Applied Mathematical Modelling, (2012).

[32] R. Hambli, Application of Neural Networks and Finite Element Computation for Multiscale Simulation of Bone Remodeling, Journal of Biomechanical Engineering, 132 (2010) 114502-114502.

[33] R. Hambli, Numerical procedure for multiscale bone adaptation prediction based on neural networks and finite element simulation, Finite elements in analysis and design, 47 (2011) 835-842.

[34] R. Hambli, Apparent damage accumulation in cancellous bone using neural networks, Journal of the mechanical behavior of biomedical materials, 4 (2011) 868-878.

[35] C.K. Fitzpatrick, M.A. Baldwin, P.J. Rullkoetter, P.J. Laz, Combined probabilistic and principal component analysis approach for multivariate sensitivity evaluation and application to implanted patellofemoral mechanics, Journal of biomechanics, 44 (2011) 13-21.

[36] R.L. Iman, Latin hypercube sampling (Wiley Online Library, 2008).

[37] J.P. Halloran, A.J. Petrella, P.J. Rullkoetter, Explicit finite element modeling of total knee replacement mechanics, Journal of biomechanics, 38 (2005) 323-331.

[38] A. Godest, M. Beaugonin, E. Haug, M. Taylor, P. Gregson, Simulation of a knee joint replacement during a gait cycle using explicit finite element analysis, Journal of biomechanics, 35 (2002) 267-275.

[39] L.A. Knight, S. Pal, J.C. Coleman, F. Bronson, H. Haider, D.L. Levine, M. Taylor, P.J. Rullkoetter, Comparison of long-term numerical and experimental total knee replacement wear during simulated gait loading, Journal of biomechanics, 40 (2007) 1550-1558.

[40] P.J. Laz, S. Pal, A. Fields, A.J. Petrella, P.J. Rullkoetter, Effects of knee simulator loading and alignment variability on predicted implant mechanics: a probabilistic study, Journal of orthopaedic research, 24 (2006) 2212-2221.

[41] S. Pal, H. Haider, P.J. Laz, L.A. Knight, P.J. Rullkoetter, Probabilistic computational modeling of total knee replacement wear, Wear, 264 (2008) 701-707.

[42] M. Van Houtem, R. Clough, A. Khan, M. Harrison, G. Blunn, Validation of the soft tissue restraints in a force-controlled knee simulator, Proceedings of the Institution of Mechanical Engineers, Part H: Journal of Engineering in Medicine, 220 (2006) 449-456.

[43] P.S. Walker, G.W. Blunn, D.R. Broome, J. Perry, A. Watkins, S. Sathasivam, M.E. Dewar, J.P. Paul, A knee simulating machine for performance evaluation of total knee replacements, Journal of Biomechanics, 30 (1997) 83-89.

[44] I. Standard, 14243-2, Wear of total knee-joint prostheses. Part 2. Methods of measurement, International Standards Organization, (2000).

[45] M.M. Ardestani, X. Zhang, L. Wang, Q. Lian, Y. Liu, J. He, D. Li, Z. Jin, Human lower extremity joint moment prediction: A wavelet neural network approach, Expert Systems with Applications, 41 (2014) 4422-4433.

[46] M.M. Ardestani, Z. Chen, L. Wang, Q. Lian, Y. Liu, J. He, D. Li, Z. Jin, A neural network approach for determining gait modifications to reduce the contact force in knee joint implant, Medical Engineering & Physics.

[47] M.M. Ardestani, Z. Chen, L. Wang, Q. Lian, Y. Liu, J. He, D. Li, Z. Jin, Feed forward artificial neural network to predict contact force at medial knee joint: Application to gait modification, Neurocomputing, 139 (2014) 114-129.

[48] A.R. Barron, Universal approximation bounds for superpositions of a sigmoidal function, Information Theory, IEEE Transactions on, 39 (1993) 930-945.

[49] E. Alpaydin, Introduction to Machine Learning (Adaptive Computation and Machine Learning Series), (The MIT Press Cambridge2004).

[50] I. Jolliffe, Principal component analysis (Wiley Online Library, 2005).

[51] B.J. Fregly, W.G. Sawyer, M.K. Harman, S.A. Banks, Computational wear prediction of a total knee replacement from in vivo kinematics, Journal of Biomechanics, 38 (2005) 305-314.

[52] C.K. Fitzpatrick, C.W. Clary, P.J. Laz, P.J. Rullkoetter, Relative contributions of design, alignment, and loading variability in knee replacement mechanics, Journal of Orthopaedic Research, 30 (2012) 2015-2024.

[53] C.K. Fitzpatrick, C.W. Clary, P.J. Rullkoetter, The role of patient, surgical, and implant design variation in total knee replacement performance, Journal of biomechanics, 45 (2012) 2092-2102.

Table 1 Geometric design variables which were defined on medial and lateral sides of the implant.

| | **Geometric variable** | **Description** | **Minimum (mm)** | **Maximum (mm)** |
|---|---|---|---|---|
| P1 | TP | Tibia posterior radius | 14 | 20 |
| P2 | TD | Tibia distal radius | 25 | 50 |
| P3 | TA | Tibia anterior radius | 15 | 70 |
| P4 | TF | Tibia frontal radius | 25 | 50 |
| P5 | FP | Femoral posterior radius | 25 | 50 |
| P6 | FD | Femoral distal radius | 5 | 9 |
| P7 | FF | Femoral frontal radius | 15 | 70 |
| P8 | W | Condylar space | 5 | 9 |

**Table(s)**

Table 2 FFANN with fifteen hidden neurons achieved the best compromise between accuracy and generality and was used in the rest of study (highlighted in gray)

| **Error goal** | | **Number of hidden units** | | | | | |
|---|---|---|---|---|---|---|---|
| | | 5 | 10 | 15 | 20 | 25 | 30 |
| E=0.01 | Accuracy | 0.79 | 0.83 | 0.89 | 0.91 | 0.96 | 0.98 |
| | Generality | 0.54 | 0.51 | 0.44 | 0.42 | 0.40 | 0.36 |
| | Epochs | 800 | 830 | 900 | 950 | 1100 | 1200 |
| E=0.05 | Accuracy | 0.73 | 0.79 | 0.88 | 0.90 | 0.94 | 0.97 |
| | Generality | 0.66 | 0.62 | 0.58 | 0.51 | 0.48 | 0.45 |
| | Epochs | 770 | 820 | 840 | 900 | 970 | 1000 |
| E=0.1 | Accuracy | 0.65 | 0.74 | 0.85 | 0.90 | 0.94 | 0.96 |
| | Generality | 0.90 | 0.95 | 1 | 1 | 1 | 1 |
| | Epochs | 660 | 600 | 580 | 520 | 500 | 460 |
| E=0.2 | Accuracy | 0.63 | 0.70 | 0.79 | 0.86 | 0.89 | 0.91 |
| | Generality | 0.91 | 0.98 | 1 | 1 | 1 | 1 |
| | Epochs | 600 | 540 | 520 | 490 | 460 | 410 |

**Figure(s)**

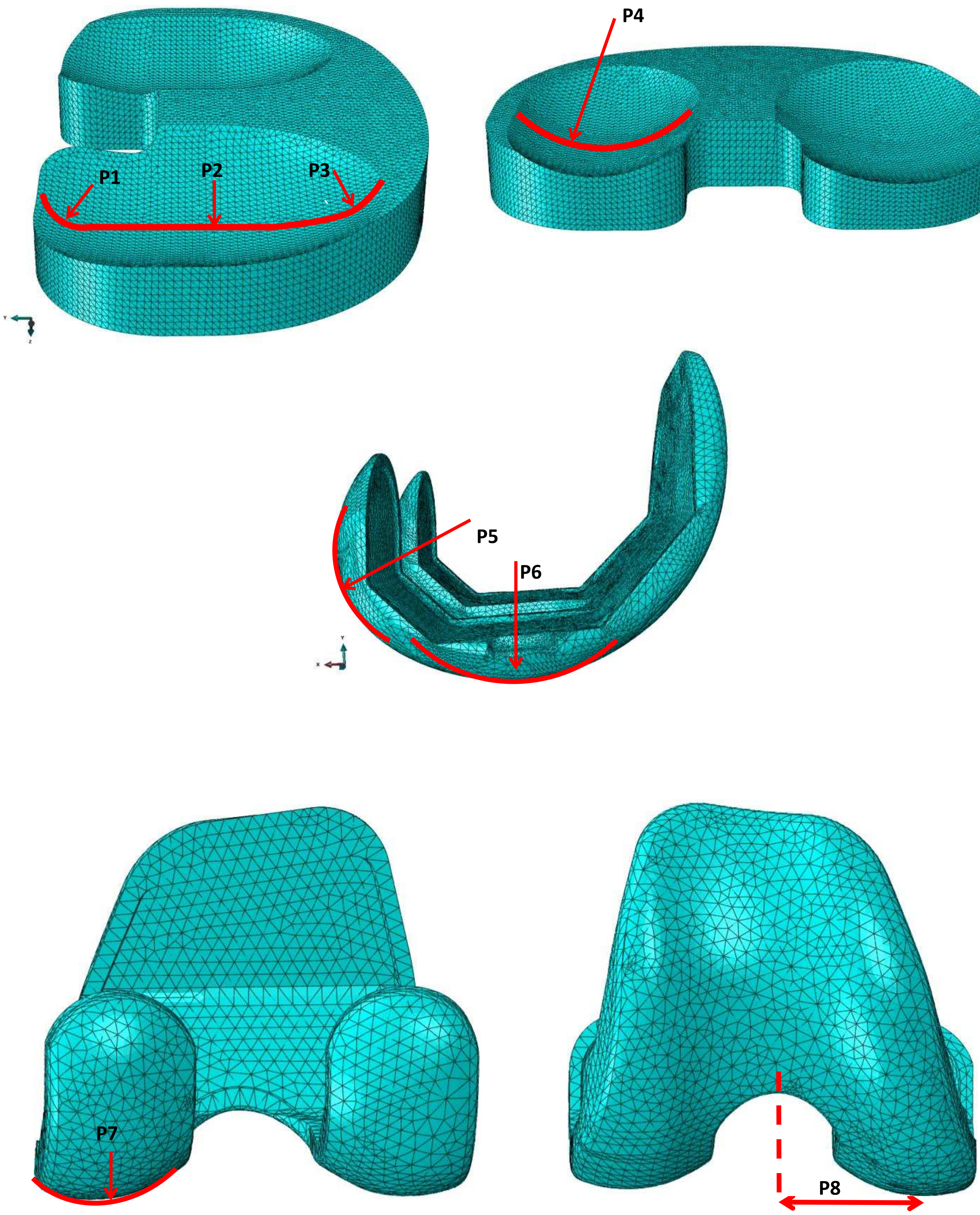


Figure 1 Geometric design variables

Figure(s)

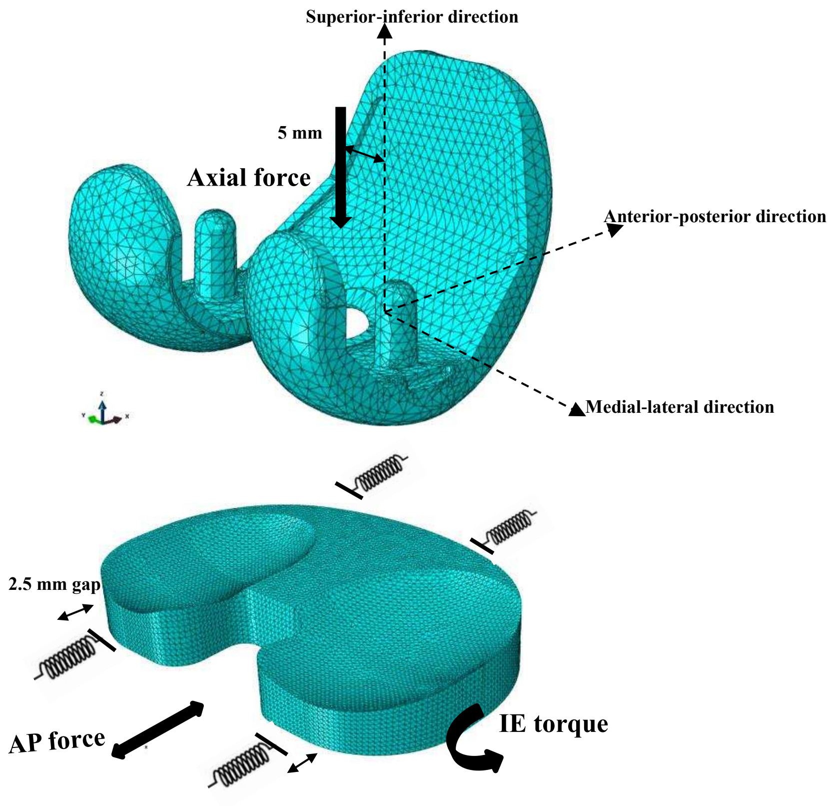


Figure 2 Finite element model of load-controlled Stanmore knee simulator

Figure(s)

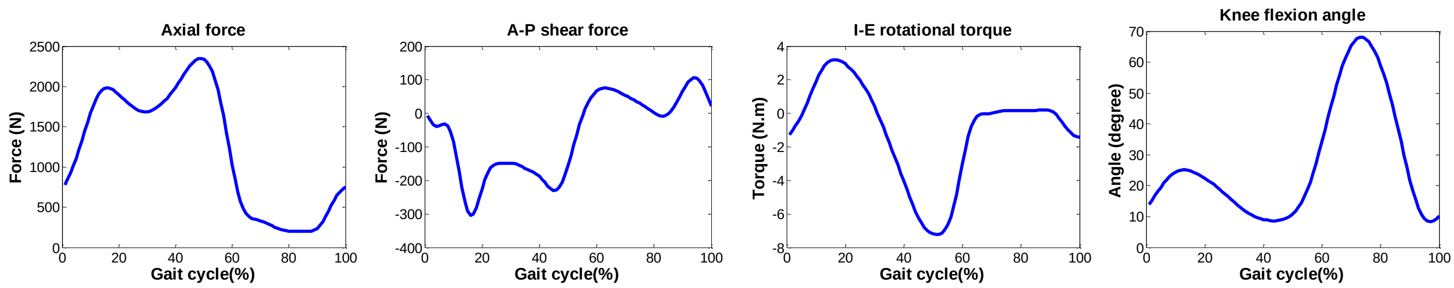


(a)

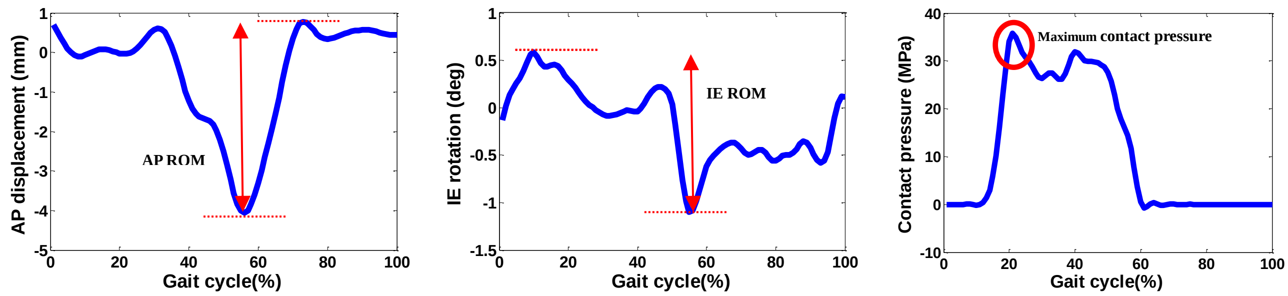


(b)

Figure 3(a) Boundary conditions and loads for FE simulation, (b) kinematic range of motion and maximum contact pressure over the entire gait cycle obtained from FE simulation

**Figure(s)**

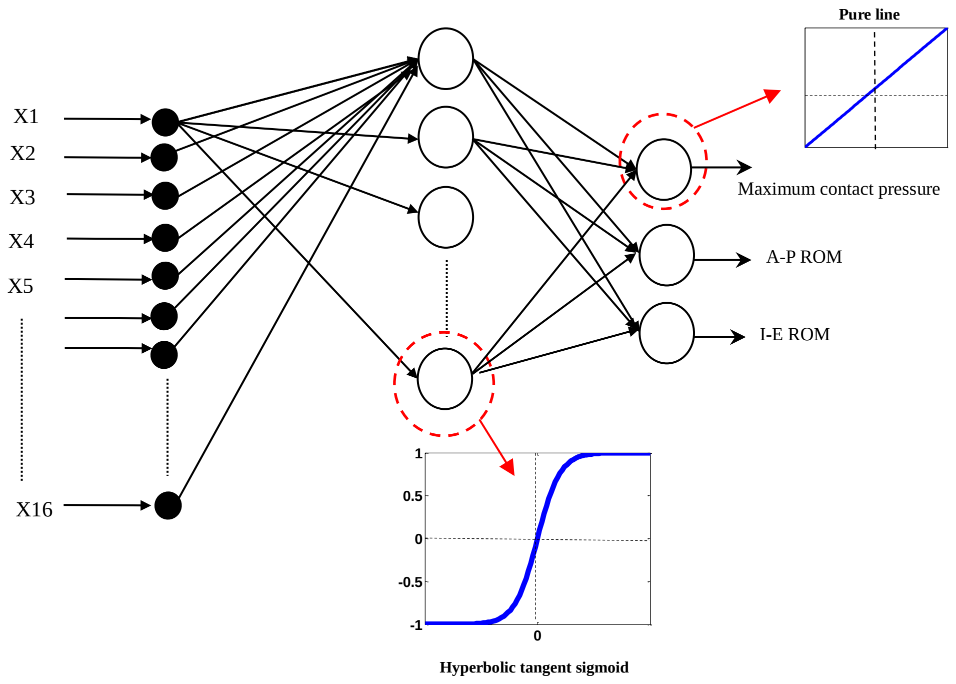


Figure 4 A schematic diagram of the proposed three-layer FFANN with sixteen input nodes (geometric variables) and three output nodes (maximum contact pressure, A-P ROM and I-E ROM)

**Figure(s)**

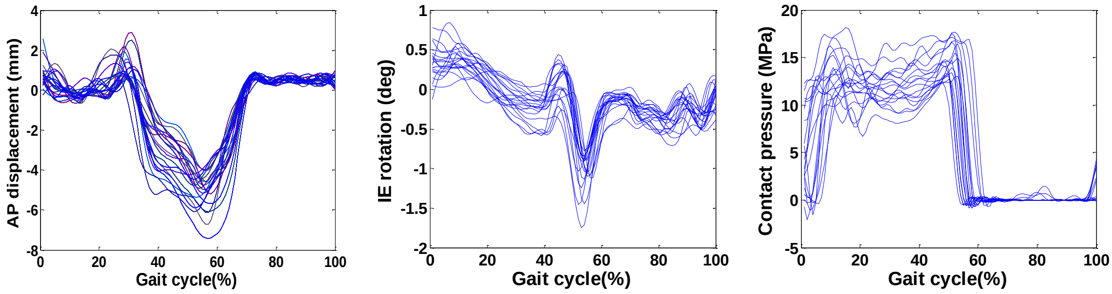


Figure 5 Contact pressure, A-P displacement and I-E rotation computed through FE simulation for a number of candidate implants.

Figure(s)

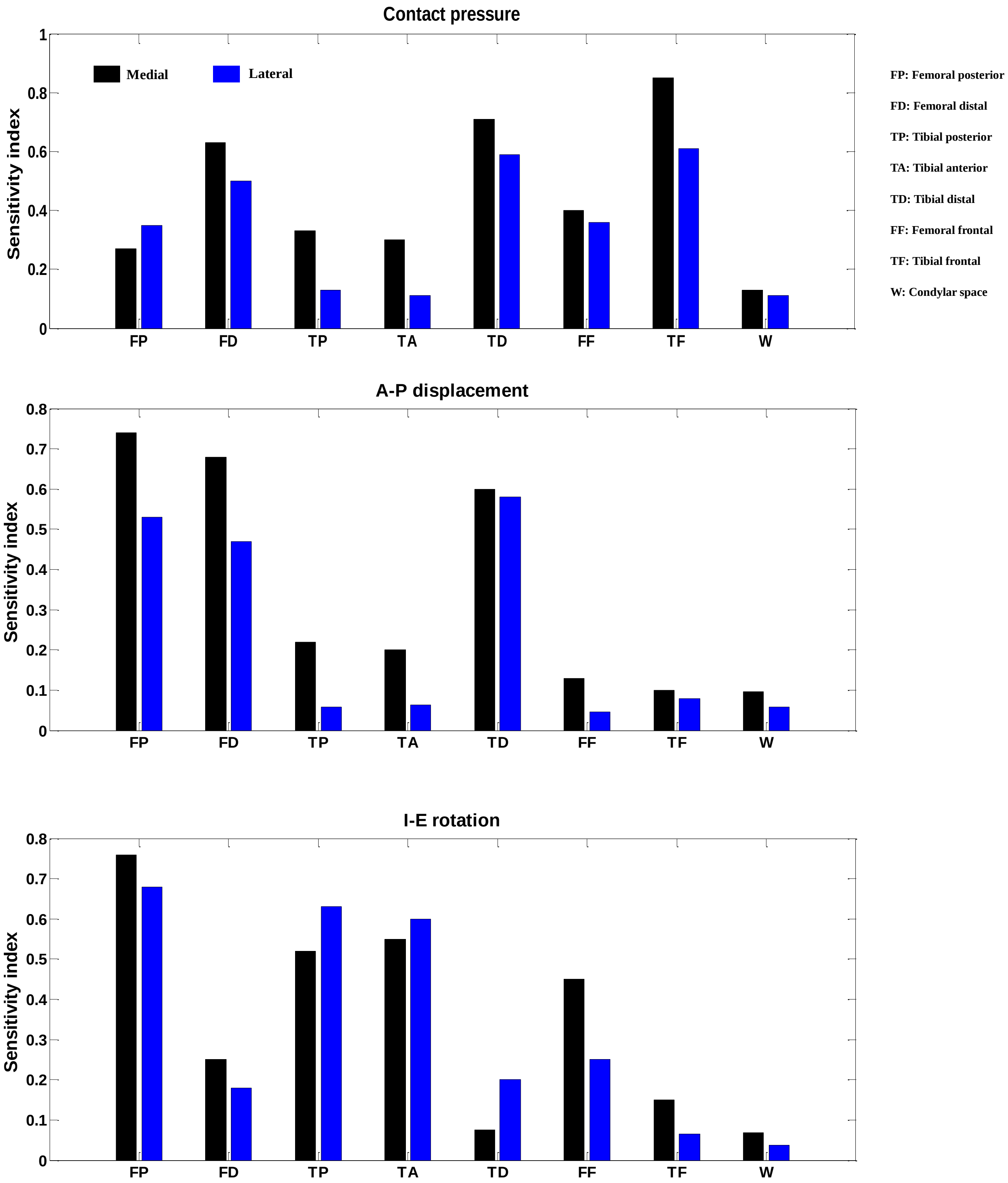


Figure 6 Sensitivity of TKA function due to individual geometric variables

## Suggested reviewers

**Professor Michael Hahn**

Department of Human Physiology

122 Esslinger Hall, 1240 University of Oregon, Eugene, OR 97403

Phone: (541) 346-3554|

Fax: 541-346-2841

Email: mhahn@uoregon.edu

**Professor Benjamin J. Fregly**

Mechanical & Aerospace Engineering Department

MAEA 208 P.O. Box 116250 Gainesville, FL 32611

Telephone: (352) 392-8157

Fax: (352) 392-7303

Email: fregly@ufl.edu

**Professor Markus A. Wimmer**

Director, Section of Tribology

Rush University Medical Center

1611 W. Harrison St., Suite 204

Chicago, IL-60612

Phone: 312-942 2789

Email: Markus_A_Wimmer@rush.edu